universe

IMPACT FACTOR 2.5

CITESCORE 4.3

Article

Primordial Axion Stars and Galaxy Halo Formation

Alexander I. Nesterov

Special Issue
Dark Energy and Dark Matter

Edited by
Prof. Dr. Yan Gong

MDPI

https://doi.org/10.3390/universe10090369

universe

MDPI

Article

Primordial Axion Stars and Galaxy Halo Formation

Alexander I. Nesterov

Department of Physics, CUCEI, University of Guadalajara, Guadalajara 44430, Jalisco, Mexico; nesterov@academicos.udg.mx

Abstract: Primordial axion stars, hypothetical stars formed from axions, could play an essential role in forming galaxy halos. These stars could have originated in the early universe shortly after the Big Bang. We show that the ultralight axions forming primordial stars can act as the initial seeds for galaxy halos.

Keywords: dark matter; axions; axion stars

1. Introduction

The axions are one of the favorite cold dark matter (CDM) candidates [1–9]. Initially, they were invented to solve the strong CP problem: Why does quantum chromodynamics (QCD) not break the CP-symmetry? The Peccei–Quinn (PQ) theory, solving this problem, leads to the existence of very light axions [10–13]. Since the axions have a tiny mass and extraordinarily weak coupling to matter and radiation, it would be challenging to detect them. Efforts toward detecting axions include a wide range of technologies [14–17].

The massless axion arises due to a spontaneous breaking of the $\mathrm{U}(1)_{\mathrm{PQ}}$ symmetry. The axion acquires a mass during the QCD phase-transition, following the PQ phase-transition. In terms of the axion decay constant, f_a, the axion mass induced by QCD instantons can be written as $m_a \approx 6\,\mu\mathrm{eV}\left(10^{12}\,\mathrm{GeV}/f_a\right)$ [12,13,18–20]. More precise estimation of the axion mass yields [21]

$$m_a \approx 5.7\,\mu\mathrm{eV}\left(\frac{10^{12}\,\mathrm{GeV}}{f_a}\right). \tag{1}$$

Cosmological and astrophysical constraints restrict the value of the decay constant and leave the allowed QCD axion mass window as $6\,\mu\mathrm{eV} \leqslant m \leqslant 2000\,\mu\mathrm{eV}$ [8,22,23]. Recent calculations of the axion mass, based on high-temperature lattice QCD, lead to the more narrow window: $50\,\mu\mathrm{eV} \leqslant m_a \leqslant 1.5\times10^3\,\mu\mathrm{eV}$ [24].

There are two sources of cold light axions: vacuum misalignment and string decay and domain-wall decay [19,25–27]. In the first case, inflation occurs after the PQ phase transition. The axion field is homogenized over enormous distances, and the vacuum misalignment yields axions with the zero-momentum mode and zero velocity dispersion. In the second scenario, the axion field will have random values in different causally connected universe volumes when the PQ phase transition occurs after inflation. This results in the appearance of a network of cosmic strings. The strings disappear after the QCD phase transition, radiating massive axions with momentum of order the Hubble expansion rate. The cold LAs, produced by string decay, have a wide distribution of momentums in their vacuum state and an extremely small velocity dispersion of their excitations [28]. The numerical lattice simulations show that the mass of QCD axions produced in the post-inflationary scenario is restricted to $0.5\,\mathrm{meV} \lesssim m_a \lesssim 20\,\mathrm{meV}$ [27]. Recent studies refine this result, leading to axion's mass prediction in the range $40\,\mu\mathrm{eV} \lesssim m_a \lesssim 180\,\mu\mathrm{eV}$ [26].

Primordial axion stars formed by QCD axions with mass $m_a \sim 10^{-6}$ eV, also known as axion clumps, are formed in the early universe shortly after the Big Bang when axions

check for updates

Citation: Nesterov, A.I. Primordial Axion Stars and Galaxy Halo Formation. *Universe* **2024**, *10*, 369. https://doi.org/10.3390/universe10090369

Academic Editor: Yan Gong

Received: 1 August 2024
Revised: 9 September 2024
Accepted: 9 September 2024
Published: 12 September 2024

condensed into a dense, gravitationally bound Bose–Einstein condensate. These clumps can range in size and mass, potentially forming compact objects with significant gravitational influence [29–35].

The axions with the mass range $10^{-33}\,\mathrm{eV} \lesssim \mathrm{m_a} \lesssim 10^{-18}\,\mathrm{eV}$, known as ultralight axions (ULA's), are considered promising candidates for dark matter [36–41]. The mass of ULA's can be estimated as follows [40,41]:

$$m_a = 5.3 \times 10^{-19}\,\mathrm{eV}\left(\frac{10^{16}\,\mathrm{GeV}}{f_a}\right)^4. \tag{2}$$

Current analyses of the Lyman-alpha forest data have placed the following lower bounds on the mass of scalar DM: $m \gtrsim 10^{-21}\,\mathrm{eV}$. Masses below this threshold would result in a universe with insufficient small-scale structure compared to what is observed [42–44].

In the modern understanding of galaxy formation, every galaxy forms within a dark matter halo. The formation of galaxy halos is a critical aspect of galaxy formation, providing the gravitational scaffold around which baryonic matter (ordinary matter) accumulates to form stars and galaxies. Primordial axion stars, formed in the early universe, could act as seeds for the formation of larger structures, leading to the formation of galaxies surrounded by halos. Their gravitational influence would attract surrounding dark matter and baryonic matter, facilitating the growth of density perturbations that eventually led to galaxy formation [45].

In this paper, we study the formation of the DM stars by ULAs and the relationship between primordial axion stars and galaxy halos. The essential features of our approach, which distinguish it from others, are the following: (1) We assume that primordial axion stars were formed in the early universe considerably before the galaxies' formation. (2) The axion density does not vanish at infinity (a usual boundary condition in previous studies). We assume that the star shell's density equals the average density of the DM.

We show that ULA stars, with a size and mass comparable with observable data for typical galaxies of our universe, are formed in the radiation-dominated era. Our findings reveal that primordial axion stars could act as the initial seeds for galaxy halos. The suggested model predicts the formation of solitonic cores surrounded by extended halos. Another feature is the formation of clusters, with a significant density, that have not merged at the center. It can explain why some dwarf spheroidal galaxies contain globular clusters.

The paper is organized as follows. Section 1 discusses the cosmological production of axions and the formation of axion stars. In Section 2, we introduce a non-relativistic model describing axion stars. Section 3 discusses the obtained results. In Conclusion, we summarize the findings of our model and future perspectives. We use the natural unit convention, $\hbar = c = 1$, throughout the paper.

2. Cosmological Production of Axions

We assume the universe is described by the ΛCDM model [46,47]. In this model, the universe comprises photons, neutrinos, ordinary (baryon) matter, cold dark matter, and dark energy. The latter is defined by the cosmological constant, Λ, and is responsible for the observable acceleration in the expansion of our universe. The axion DM can be described by a model with the action given by [19,38,40]

$$S = \int \sqrt{-g}\, d^4x \left(\frac{1}{2} g^{\mu\nu}\phi_{,\mu}\phi_{,\nu} - V(\phi)\right). \tag{3}$$

The corresponding equation of motion is the Klein–Gordon equation:

$$\Box\phi = -\frac{\partial V(\phi)}{\partial \phi}. \tag{4}$$

Qualitatively, the potential $V(\phi)$ generated by QCD instantons may be written as [11,19]

$$V(\phi) = (m_a f_a)^2 \Big(1 - \cos(\phi/f_a)\Big), \tag{5}$$

where m_a is the axion mass. The potential $V(\phi)$ is the periodic function with a period defined by a shift-invariance, $\phi \to \phi + 2\pi f_a$. There are N degenerate vacua, and the axion field has a range $0 < \phi < 2\pi f_a$ [19].

2.1. Non-Relativistic Limit of the Klein–Gordon Equation

In the non-relativistic limit, the Klein–Gordon equation has the form of the Schrödinger equation with the effective potential describing the interacting forces in the system in the non-relativistic limit [29,30,48–50]. By writing

$$\phi = \frac{1}{2\sqrt{m_a}} \left(\psi e^{-i m_a t} + \psi^* e^{i m_a t} \right), \tag{6}$$

one can show that the non-relativistic theory is described by the effective action for the complex field ψ:

$$S_{\text{eff}} = \int d^4x \Big(\frac{i}{2}(\psi^* \dot{\psi} - \dot{\psi}^* \psi) - \frac{1}{2m_a} \nabla\psi^* \cdot \nabla\psi - V_{\text{eff}}(\psi^*\psi) - \frac{1}{8\pi G} \nabla\Phi \cdot \nabla\Phi - m_a \psi^* \psi \Phi \Big), \tag{7}$$

where $\Phi(\mathbf{r})$ is the Newtonian gravitational potential, and $V_{eff}(|\psi|)$ is the effective potential obtained as the non-relativistic limit of the instanton potential Equation (5). The equations of motion are given by

$$\begin{aligned} i\frac{\partial \psi}{\partial t} &= -\frac{1}{2m} \nabla^2 \psi + m_a \Phi \psi + \frac{\partial V_{\text{eff}}}{\partial \psi^*} \psi, \\ \nabla^2 \Phi &= 4\pi G m_a |\psi|^2. \end{aligned} \tag{8}$$

For the axion field, the effective instanton non-relativistic potential potential was derived in Refs. [48,51] and takes the form

$$V_{\text{eff}}\left(\psi^*\psi\right) = \frac{1}{2} m_a \psi^* \psi + m_a^2 f_a^2 \left[1 - J_0\left(n^{1/2}\right) \right], \tag{9}$$

where $J_0(z)$ is a Bessel function, $n = \psi^*\psi/n_0$ and $n_0 = m_a f_a^2/2$.

Figure 1 represents the normalized effective potential, $V_0(x) = 1 - J_0(x)$, with the first term subtracted:

$$V_0 = \frac{1}{2 m n_0} \left(\mathcal{V}_{\text{eff}} - \frac{1}{2} m_a \psi^* \psi \right) \tag{10}$$

The stable solutions for the axion stars with $n \gg 1$ (dense stars) correspond to the minima of the effective potential [29].

2.2. Formation of Axion Stars

Axion stars are characterized by their high density and stability, maintained by a balance between gravitational attraction and quantum pressure due to the axions' wave-like nature. They can be categorized into two types:

- **Dilute Axion Stars** ($n_{core} \ll 1$). These stars are less dense and more extended, and their size is determined by the axion mass and self-interaction strength.
- **Dense Axion Stars** ($n_{core} \gg 1$). These are more compact and can undergo complex dynamical processes, including potential collapse into black holes and phase transition to the dilute stars under certain conditions.

The stability and structure of axion stars are determined by the balance between gravitational attraction and the quantum pressure arising from the Heisenberg uncertainty principle.

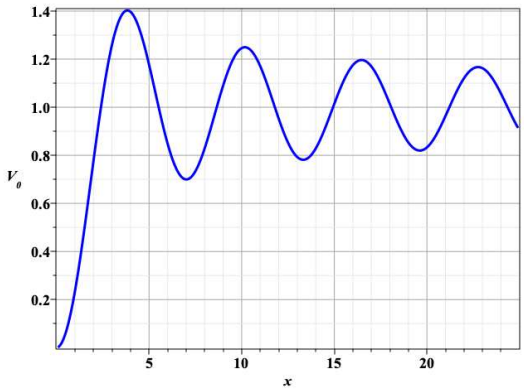

Figure 1. Effective potential: $V_0 = 1 - J_0(x)$.

3. Model

The non-relativistic axions can form a Bose–Einstein condensate (BEC). The equations that describe a static BEC of axions can be obtained by considering an axion field $\psi(\boldsymbol{r}, t)$ whose time dependence is $\psi(\boldsymbol{r}) \exp(-i\mu t)$, where μ is the chemical potential [29]. They can be expressed conveniently as coupled equations for $\psi(\boldsymbol{r})$ and the gravitational potential $\Phi(\boldsymbol{r})$:

$$\begin{aligned} \nabla^2\hat{\psi} =& 2m_a^2\left(\Phi - \frac{\mu}{m_a} - \frac{1}{2} + \frac{J_1(|\hat{\psi}|)}{|\hat{\psi}|}\right)\hat{\psi}, \\ \nabla^2\Phi =& 4\pi G m_a n_0 |\hat{\psi}|^2, \end{aligned} \tag{11}$$

where $\hat{\psi} = \psi/\sqrt{n_0}$, $G = 1/m_p^2$, and m_p denotes the Planck mass ($m_p = 1.2 \times 10^{19}$ GeV). To further simplify matters, we rescale coordinates and functions: $\boldsymbol{r} \to \boldsymbol{r}^* = \boldsymbol{r}/r_0$, $\psi \to \psi(\boldsymbol{r}^*)$ and $\Phi \to \gamma\Phi(\boldsymbol{r}^*)$, where $r_0 = \gamma/m_a$ and $\gamma = m_p/f_a$.

Hereafter, we drop the $*$'s in rescaled functions and coordinates. Then, the dimensionless equations can be recast as follows:

$$\begin{aligned} \nabla^2\hat{\psi} =& 2\Big(\Phi - \gamma\varepsilon\Big)\hat{\psi}, \\ \nabla^2\Phi =& 4\pi|\hat{\psi}|^2, \end{aligned} \tag{12}$$

where

$$\varepsilon = \bar{\mu} + \frac{1}{2} - \frac{J_1(|\hat{\psi}|)}{|\hat{\psi}|}, \tag{13}$$

and we set $\bar{\mu} = \mu/m_a$.

In Table 1, we present various length and mass scales to facilitate recalculation in physical units. In particular, the mass of the axion star can be obtained using the following formula:

$$M = 3\, M_0 \int |\hat{\psi}|^2 d^3V^*, \tag{14}$$

where $M_0 = 4\pi m_a n_0 r_0^3/3$, and the integration is performed over dimensionless variables.

Table 1. Acronyms: f_a—coupling constant; $M_\odot$—sun mass; n_{DM}—particle DM density.

Axion Mass [eV]	f_a **[GeV]**	r_0 **[pc]**	M_0 $[M_\odot]$	n_0 $[1/cm^3]$	$n^* = n_{DM}/n_0$
10^{-21}	4.8×10^{16}	1.6	6.86×10^{13}	1.5×10^{44}	8.67×10^{-21}
5.3×10^{-19}	10^{16}	1.448×10^{-2}	3.59×10^{8}	3.45×10^{45}	7.11×10^{-23}

Our model is based on the previous studies of the rotating axion stars made in [29,31,32,49,52]. In general ψ may consist of a superposition of spherical harmonics Y_l^m,

$$\hat{\psi}(r,\theta,\varphi) = \sum_{\ell=0}^{\infty} \sum_{m=-l}^{\ell} f_\ell^m r^\ell Y_\ell^m(\theta,\varphi). \tag{15}$$

For simplicity, we assume the following ansatz:

$$\hat{\psi}(r,\theta,\phi) = R(r) Y_l^m(\theta,\varphi). \tag{16}$$

After substitution of $\hat{\psi}(r,\theta,\phi)$, one can rewrite Equation (12) as

$$\begin{aligned} &\Delta_r R - \frac{l(l+1)}{r^2} R = 2\left(\Phi - \gamma\bar{\mu} - \frac{\gamma}{2} + \frac{\gamma J_1(R|Y_l^m|)}{R|Y_l^m|}\right) R, \\ &\nabla^2\Phi = 4\pi R^2 |Y_l^m|^2, \end{aligned} \tag{17}$$

where Δ_r denotes the radial part of the Laplacian,

$$\Delta_r = \frac{1}{r^2}\frac{\partial}{\partial r}\left(r^2 \frac{\partial}{\partial r}\right). \tag{18}$$

Note that (17) still depends on angular variables θ and φ. Following the procedure presented in [49], we take the angular average of these equations to obtain the following equations of motion:

$$\Delta_r R = 2\left(\tilde{\Phi} + \frac{l(l+1)}{2r^2} - \gamma\bar{\mu} - \frac{\gamma}{2} + \gamma\mathcal{J}_l^m)\right) R, \tag{19}$$

$$\Delta_r \tilde{\Phi} = R^2, \tag{20}$$

where

$$\tilde{\Phi} = \frac{1}{4\pi}\int \Phi(r,\theta,\varphi) d\Omega, \quad \mathcal{J}_l^m = \frac{1}{4\pi}\int \frac{J_1(R|Y_l^m|)}{R|Y_l^m|} d\Omega. \tag{21}$$

We used the normalization of the spherical harmonics, $\int Y_\ell^m Y_{\ell'}^{m'*} d\Omega = \delta_{\ell\ell'}\delta_{mm'}$, to perform averaging. For $l = 0, 1$, we have obtained the analytical expressions for $\mathcal{J}_l^m$:

$$\mathcal{J}_1^0 = J_0(a_0 R) - \frac{J_1(a_0 R)}{a_0 R} + \frac{\pi}{2}\Big(J_1(a_0 R)H_0(a_0 R) - J_0(a_0 R)H_1(a_0 R)\Big), \tag{22}$$

$$\mathcal{J}_1^{\pm 1} = \frac{1-\cos(a_1 R)}{a_1^2 R^2}, \quad \mathcal{J}_0^0 = \frac{J_1(R)}{R}, \tag{23}$$

where $a_0 = \sqrt{3/4\pi}$, $a_1 = \sqrt{3/8\pi}$ and $H_n(z)$ denotes the Struve function.

For a given function $R(r)$, the gravitational potential can be obtained by integrating Equation (20). The solution can be written as follows:

$$\tilde{\Phi}(r) = -\frac{1}{r}\int_0^r x^2 R^2(x) dx - \int_r^{r_h} x R^2(x) dx, \tag{24}$$

where r_h is the radius of the star. From here it follows that $\tilde{\Phi}(0) = \tilde{\Phi}_0$ and $\Phi'(0) = 0$, where

$$\tilde{\Phi}_0 = -\int_0^{r_h} xR^2(x)dx. \tag{25}$$

We impose the following boundary conditions to solve numerically the coupling system of the differential Equations (19) and (20):

$$R(0) = R_0, \quad R(0)' = R_1, \quad \tilde{\Phi}(0) = \Phi_0, \quad \tilde{\Phi}'(0) = 0. \tag{26}$$

The radius of the axion star is obtained as the solution of the equation

$$\tilde{\Phi}(r_h) = -\frac{M^*(r_h)}{r_h}, \tag{27}$$

where $M^*(r_h) = \int_0^{r_h} x^2R^2(x)dx$ is the rescaled mass of the star, $M^* = M/M_0$, and

$$\tilde{\Phi}(r_h) = -\frac{1}{r_h}\int_0^{r_h} x^2R^2(x)dx. \tag{28}$$

The chemical potential is subject to the following boundary conditions:

$$\bar{\mu} = \left[\frac{1}{\gamma}\left(\tilde{\Phi} + \frac{l(l+1)}{2r^2}\right) + \mathcal{J}_l^m - \frac{1}{2}\right]\Bigg|_{r=r_h} = 0 \tag{29}$$

Redshift and universe chronology. The redshift for different stages of the universe's evolution can be estimated as follows:

- Energy-dominated era: $z = (0 - 1.46)$
- Matter-dominated era: $z = (1.46 - 4.86 \times 10^3)$
- Radiation-dominated era: $z = (4.86 \times 10^3 - 5.92 \times 10^{15})$

We use the ΛCDM model [46,47] to estimate the redshift. For the dark energy-dominated era, the redshift is given by

$$1 + z = \frac{a(t)}{a(t_m)} = \frac{\sinh^{2/3}\left(\frac{3}{2}H_0\sqrt{\Omega_\Lambda}\,t\right)}{\sinh^{2/3}\left(\frac{3}{2}H_0\sqrt{\Omega_\Lambda}\,t_m\right)}, \tag{30}$$

where $\Omega_\Lambda = \Lambda/(3H_0^2)$, and H_0 is the Hubble constant. This expression is quite accurate for $t > t_m = 10\,\mathrm{Myr}(10^7\,\mathrm{y}) = 3.15 \times 10^{14}$ s. For a radiation-dominated era, we have $a(t) \propto \sqrt{t}$, and for a matter-dominated universe, $a(t) \propto t^{2/3}$. Combining all results, we obtain

$$z \approx \sqrt{\frac{t_r}{t_i}}\left(\frac{t_m}{t_r}\right)^{2/3} \frac{\sinh^{2/3}\left(\frac{3}{2}H_0\sqrt{\Omega_\Lambda}\,t\right)}{\sinh^{2/3}\left(\frac{3}{2}H_0\sqrt{\Omega_\Lambda}\,t_m\right)}. \tag{31}$$

For an estimation, we take the following values: $t_m = 9$ billion years (end of the matter-dominated era and beginning of the dark energy-dominated era), $t_r = 47,000$ years (end of the radiation-dominated era), and $t_i = 10^{-12}$ s (beginning of the radiation-dominated era).

4. Results and Discussion

Following the procedure outlined in Section 3, we have solved numerically the equations of motion (19) and (20) for the axion mass, $m_a = 5.3 \times 10^-19$ eV, and the boundary conditions presented below.

- Dense stars

$$\begin{aligned}
&\text{DES(I))}: \quad R(0)=6, \quad R(0)'=0, \quad \tilde{\Phi}(0)=-1.5, \quad \tilde{\Phi}'(0)=0, (l=0,\, m=0),\\
&\text{DES(II))}: \quad R(0)=20, \quad R(0)'=0, \quad \tilde{\Phi}(0)=-3.15, \quad \tilde{\Phi}'(0)=0, (l=0,\, m=0).
\end{aligned}$$

- Dilute stars

$$\begin{aligned}
&\text{DIS(I))}: \quad R(0)=0.1, \quad R(0)'=0, \quad \tilde{\Phi}(0)=-0.055, \quad \tilde{\Phi}'(0)=0, (l=0,\, m=0),\\
&\text{DIS(II))}: \quad R(0)=0, \quad R(0)'=10, \quad \tilde{\Phi}(0)=-0.001, \quad \tilde{\Phi}'(0)=0, (l=1,\, m=0),\\
&\text{DIS(III)}: \quad R(0)=0, \quad R(0)'=0.12, \quad \tilde{\Phi}(0)=-0.5, \quad \tilde{\Phi}'(0)=0, (l=1,\, m=\pm 1).
\end{aligned}$$

The boundary of the star is fixed by conditions imposed by Equation (27).

The results of the numerical solution of Equations (19) and (20) are presented in Figures 2–4 and summarized in Table 2. As one can see, the axion stars have an explicitly expressed core with the radius, $r_{core} \ll r_h$. Inside the stellar shell, the density oscillates around some non-zero value. The oscillations in graphs reflect the oscillating character of the Bessel functions.

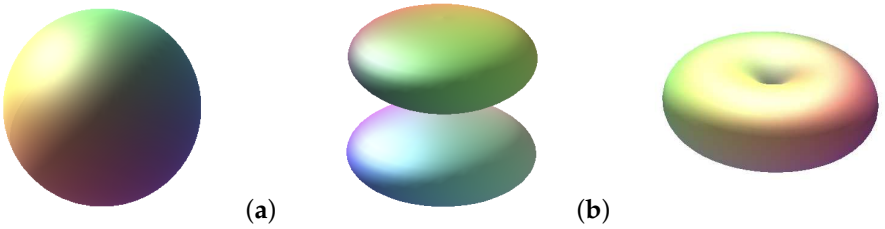

Figure 2. Angular distribution of the axion field density: (**a**) $l = 0, m = 0$; (**b**) $l = 1, m = 0$; (**c**) $l = 1, m = \pm 1$.

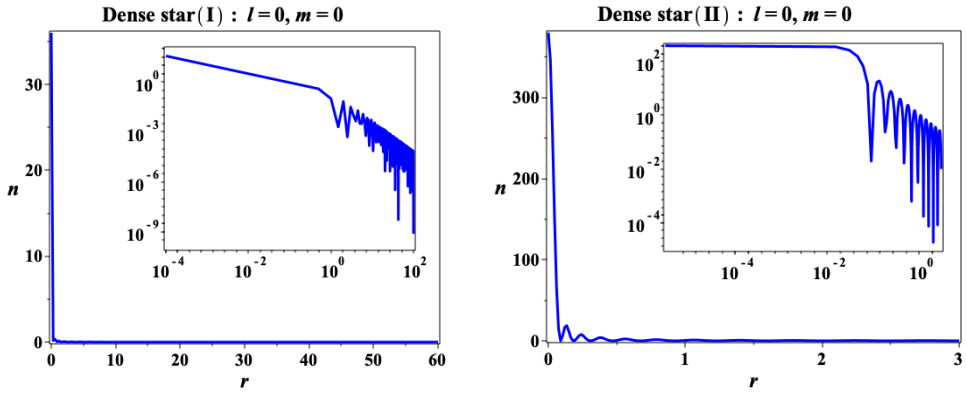

Figure 3. Dense stars. Radial distribution of the axion field density. Inset: log–log plot.

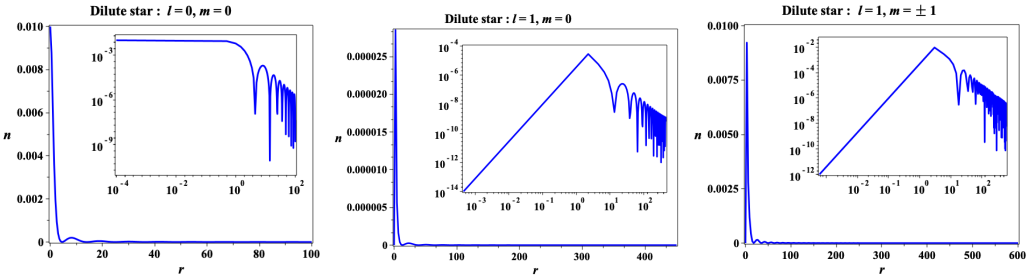

Figure 4. Dilute stars. Radial distribution of the axion field density. Inset: log–log plot.

We assume that the primordial axion stars are formed in the relatively late universe compared with the inflation and the Big Bang nucleosynthesis periods (around hours after the Big Bang). At the star's boundary, the axion particle density is $n_b = n_{DM}(z)$, where $n_{DM}(z)$ is the average particle density of DM at the redshift z. To obtain the redshift, we use the

relation, $z = (n_{DM}(z)/n_{DM})^{1/3}$, where $n_{DM} = \rho_{\rm DM}/m_a$, and $\rho_{\rm DM} = 1.3 \times 10^{-6}\,{\rm GeV/cm^3}$ is the observed average density of the DM obtained from the data presented in Ref. [53].

Table 2. Acronyms: $n_h = n_b/n_0$—normalized axion density n_b at the star's boundary to n_0. DES (I)—dense star with the boundary conditions (I); DES (II)—dense star with the boundary conditions (II); DIS (I)—dilute star with the boundary conditions (I); DIS (II)—dilute star with the boundary conditions (II); DIS (III)—dilute star with the boundary conditions (III).

Star Type	**Angular Momentum**	**Axion Mass $m_a = 5.3 \times 10^{-19}$ eV**			
		Star Radius, r_h	**Star Mass, M**	**Density, n_h**	**Redshift, z**
DES (I)	$l = 0, m = 0$	55 [0.796 pc]	43.8 [$1.57 \times 10^{10}\,M_\odot$]	5.86×10^{-6}	4.35×10^{5}
DES (II)	$l = 0, m = 0$	2.9 [0.042 pc]	5.56 [$1.99 \times 10^{9}\,M_\odot$]	0.022	6.76×10^{6}
DIS (I)	$l = 0, m = 0$	100 [1.448 pc]	2.66 [$9.56 \times 10^{8}\,M_\odot$]	4.27×10^{-8}	8.43×10^{4}
DIS (II)	$l = 1, m = 0$	410 [5.94 pc]	0.11 [$4 \times 10^{7}\,M_\odot$]	1.21×10^{-12}	2572
DIS (III)	$l = 1, m = \pm 1$	550 [7.96 pc]	109.5 [$3.92 \times 10^{10}\,M_\odot$]	1.77×10^{-11}	6291

The current size of the primordial axion stars can be estimated using the following relation: $d = 2zr_h$. We obtain

- DES (I): $d = 693.3$ kpc ($l = 0, m = 0$, $M = 1.57 \times 10^{10}\,M_\odot$)
- DES (II): $d = 567.8$ kpc ($l = 0, m = 0$, $M = 1.99 \times 10^{9}\,M_\odot$)
- DIS (I): $d = 244.3$ kpc ($l = 0, m = 0$, $M = 9.56 \times 10^{8}\,M_\odot$)
- DIS (II): $d = 30.6$ kpc ($l = 1, m = 0$, $M = 4 \times 10^{7}\,M_\odot$)
- DIS (III): $d = 100$ kpc ($l = 1, m = \pm 1$, $M = 3.92 \times 10^{10}\,M_\odot$)

These results are in agreement with an estimation of the halo size for typical galaxies:

- Spiral Galaxies: 61.3 to 92 kpc in diameter
- Elliptical Galaxies: 92 to 306.6 kpc in diameter
- Dwarf Galaxies: up to 9.2 kpc in diameter

The mass of galaxies can vary significantly depending on their type and size:

- Spiral Galaxies: $M \approx (10^{10} - 10^{12})M_\odot$.
- Elliptical Galaxies: $M \approx (10^{12} - 10^{13})M_\odot$.
- Dwarf Galaxies: $M \approx (10^{7} - 10^{9})M_\odot$.

Considering the distribution of different types of galaxies, the average mass of galaxies in our universe can be roughly estimated as follows: $M \approx 10^{11} M_\odot$. As one can see, the mass of axion stars presented in Table 2 is inside the range of the observable data. Below, we discuss these results in detail.

Elliptical galaxies. Elliptical galaxies are characterized by their ellipsoidal shape. They range from nearly spherical to highly elongated shapes. The stars in elliptical galaxies typically orbit in random directions, which contributes to their more rounded appearance. The best candidates for forming elliptical galaxies are dilute axion stars with spherical symmetry ($l = 0, m = 0$). The current size of the presented primordial axion star is an order of the visible halo of the typical elliptical galaxy. These stars are formed at the beginning of the radiation-dominated era ≈150 years after the Big Bang.

Dwarf galaxies. Dwarf galaxies are small galaxies that contain significantly fewer stars compared to giant galaxies like the Milky Way. They are among the most common types of galaxies in the universe and play a crucial role in studying galaxy formation and evolution. Dwarf galaxies are thought to be the building blocks of more giant galaxies. Over time, they can merge with one another or be absorbed by larger galaxies.

Dwarf galaxies exhibit uniform central masses and shallow density profiles that imply the density decreases slowly with distance from the center. The most crucial feature of dwarf galaxies is that, in many cases, they are often dominated by DM so that the DM mass

can be several times greater than the mass of its visible components. Dwarf galaxies can be of various types: elliptical, spheroidal, and irregular. Less common are dwarf spiral galaxies, which exhibit spiral structures.

The essential features of dwarf galaxies, like solitonic cores surrounded by extended halos, in our model are presented by spherically- symmetric primordial dense axion stars (see Figure 3). These stars are formed at the beginning of the radiation-dominated era, at high redshifts, around $z \gtrsim 6.76 \times 10^6$ (≈3.6 h after the Big Bang). In Table 3 and Figure 5, we summarize the results of the numerical solution for DES (I)—dense star with the boundary conditions (I) and DES (II)—dense star with the boundary conditions (II). The first minimum of the axion density in Figure 3 defines the radius of the star core.

Figure 5 presents the dimensionless axion field density of the star core, $\rho/\langle\rho\rangle$, where $\langle\rho\rangle$ denotes the mean density of DM. All halos demonstrate a distinct inner core with uniform central distribution of masses. Initially, both stars have close sizes. The ratio of the current sizes of star cores is ≈ 13.6 times. This significant difference is explained by different redshifts related to times of star formation: DES (I) (≈3.6 h) and DES(II) (≈5.9 h) after the Big Bang. Figure 6 shows that besides the central core, there are clusters with a significant density that have not merged at the center. It can explain why some dwarf spheroidal galaxies contain globular clusters.

Table 3. Acronyms: DES (I)—dense star with the boundary conditions (I); DES (II)—dense star with the boundary conditions (II).

Star Type	Star Core Radius, r_{core}		Star Mass	
	Initial	Current	Core Mass, M_{core}	Total Mass, M_{total}
DES (I)	1.5×10^{-3} pc	0.65 kpc	$1.4 \times 10^6\ M_\odot$	$1.57 \times 10^{10}\ M_\odot$
DES (II)	1.3×10^{-3} pc	8.81 kpc	$1.61 \times 10^7\ M_\odot$	$1.99 \times 10^9\ M_\odot$

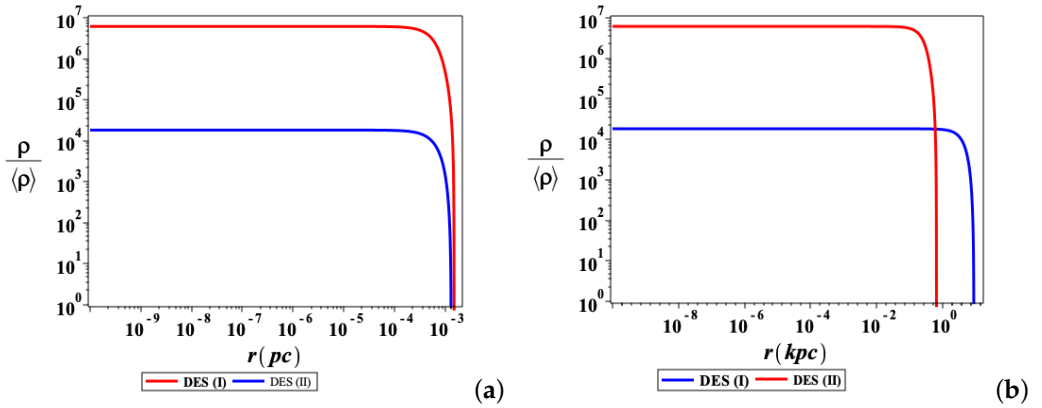

Figure 5. Log−log plot. Radial density profiles of halos normalized to the mean DM density. (**a**) Halo profiles of primordial axion stars at $z \gtrsim 6.76 \times 10^6$. (**b**) Current halo profiles. All halos possess a distinct inner core with uniform central distribution of masses.

Spiral galaxies. Spiral galaxies, one of the most common galaxies in the universe, have a complex structure consisting of a thin rotating disk and a spherical halo. According to our model, the primordial axion stars that could be seeds of spiral galaxies are the stars with angular momentum $l = 1$ and $m \pm 1$ (Figure 2c). The current size of the axion star is an order of the visible halo of the spiral galaxy. Formation of the rotating axion stars begins in the middle of the radiation-dominated era ≈ 28,000 years after the Big Bang. The axion stars with $l = 1$ and $m = 0$ are possible candidates for the formation of dwarf spiral galaxies. These stars are formed at the beginning of the matter-dominated era $\approx 1.22 \times 10^5$ years after the Big Bang.

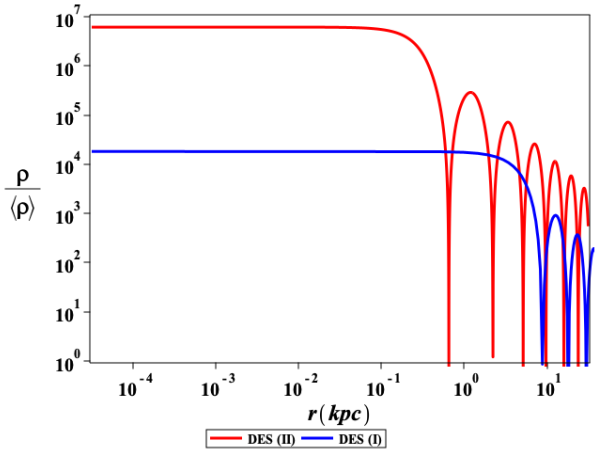

Figure 6. Log plot. Radial density profiles of halos normalized to the mean DM density. Radial density profiles of halos normalized to the mean DM density. Some clusters have not merged at the center.

Our model predicts the formation of solitonic cores surrounded by extended halos. Another feature is the formation of clusters that do not merge at the center. It can give a potential explanation for why the Fornax dwarf spheroidal galaxy, a satellite of the Milky Way, contains globular clusters [54]. Our findings qualitatively agree with the recent numerical simulations of the ψDM model presented in Refs. [55,56]. The difference is in the shape of the core profile. In our model, the central distribution of the density is uniform. The smoother density profile in the ψDM model shows a rather fast decay compared to ours. The possible explanation for this discrepancy is the complicated dynamics of the primordial axion star created in the early universe. Over time, the axion star (a dwarf galaxy in the future) could attract more matter and change its profile to the modern one. One needs a more profound study on this issue.

5. Conclusions

The suggested model assumes that ULA stars, formed in the early universe, could act as seeds for forming larger structures that would become galaxies in the future. Their gravitational field would attract surrounding DM and baryonic stars, eventually creating a galaxy.

Primordial axion stars offer potential insights into the nature of DM and its role in galaxy formation. As ULA stars attract additional axions, they contribute to the overall density of DM halos. This increased density can enhance the halo's gravitational potential, making it more effective at attracting and retaining baryonic matter. Primordial ULA stars can play a crucial role in forming the observable universe's shape by acting as seeds for galaxy formation. One needs a more profound study of UlA dynamics to make our model more realistic.

Funding: This research received no external funding.

Data Availability Statement: No new data were created or analyzed in this study.

Acknowledgments: We want to express our sincere gratitude to the referees for their valuable comments and suggestions, which significantly improved the quality of our manuscript.

Conflicts of Interest: The author declares no conflict of interest.

References

1. Preskill, J.; Wise, M.B.; Wilczek, F. Cosmology of the invisible axion. *Phys. Lett. B* **1983**, *120*, 127–132. [CrossRef]
2. Abbott, L.; Sikivie, P. A cosmological bound on the invisible axion. *Phys. Lett. B* **1983**, *120*, 133–136. [CrossRef]
3. Dine, M.; Fischler, W. The not-so-harmless axion. *Phys. Lett. B* **1983**, *120*, 137–141. [CrossRef]
4. Kawasaki, M.; Nakayama, K. Axions: Theory and Cosmological Role. *Annu. Rev. Nucl. Part. Sci.* **2013**, *63*, 69–95. [CrossRef]

5. Feng, J.L. Dark Matter Candidates from Particle Physics and Methods of Detection. *Annu. Rev. Astron. Astrophys.* **2010**, *48*, 495–545. [CrossRef]
6. Bertone, G.; Hooper, D. History of dark matter. *Rev. Mod. Phys.* **2018**, *90*, 045002. [CrossRef]
7. O'Hare, C.A.J. Cosmology of axion dark matter. In Proceedings of the 1st General Meeting and 1st Training School of the COST Action COSMIC WISPers—PoS (COSMICWISPers), Bari and Lecce, Italy, 5–14 September 2023; p. 040. [CrossRef]
8. Di Luzio, L.; Giannotti, M.; Nardi, E.; Visinelli, L. The landscape of QCD axion models. *Phys. Rep.* **2020**, *870*, 1–117. [CrossRef]
9. Chadha-Day, F.; Ellis, J.; Marsh, D.J.E. Axion dark matter: What is it and why now? *Sci. Adv.* **2022**, *8*, eabj3618. [CrossRef]
10. Peccei, R.; Quinn, H. CP Conservation in the Presence of Pseudoparticles. *Phys. Rev. Lett.* **1977**, *38*, 1440–1443. [CrossRef]
11. Peccei, R.D.; Quinn, H.R. Constraints imposed by CP conservation in the presence of pseudoparticles. *Phys. Rev. D* **1977**, *16*, 1791–1797. [CrossRef]
12. Weinberg, S. A New Light Boson? *Phys. Rev. Lett.* **1978**, *40*, 223–226. [CrossRef]
13. Wilczek, F. Problem of Strong *P* and *T* Invariance in the Presence of Instantons. *Phys. Rev. Lett.* **1978**, *40*, 279–282. [CrossRef]
14. Rosenberg, L.J. Dark-matter QCD-axion searches. *Proc. Natl. Acad. Sci. USA* **2015**, *112*, 12278–12281. [CrossRef]
15. Arvanitaki, A.; Huang, J.; Van Tilburg, K. Searching for dilaton dark matter with atomic clocks. *Phys. Rev. D* **2015**, *91*, 015015. [CrossRef]
16. Arvanitaki, A.; Dimopoulos, S.; Van Tilburg, K. Sound of Dark Matter: Searching for Light Scalars with Resonant-Mass Detectors. *Phys. Rev. Lett.* **2016**, *116*, 031102. [CrossRef]
17. Irastorza, I.G.; Redondo, J. New experimental approaches in the search for axion-like particles. *Prog. Part. Nucl. Phys.* **2018**, *102*, 89–159. [CrossRef]
18. Turner, M.S. Windows on the axion. *Phys. Rep.* **1990**, *197*, 67–97. [CrossRef]
19. Sikivie, P. Axion Cosmology. In *Axions: Theory, Cosmology, and Experimental Searches*; Kuster, M., Raffelt, G., Beltrán, B., Eds.; Springer: Berlin/Heidelberg, Germany, 2008; pp. 19–50.
20. Chang, S.; Hagmann, C.; Sikivie, P. Studies of the motion and decay of axion walls bounded by strings. *Phys. Rev. D* **1998**, *59*, 023505. [CrossRef]
21. di Cortona, G.G.; Hardy, E.; Vega, J.P.; Villadoro, G. The QCD axion, precisely. *J. High Energy Phys.* **2016**, *2016*, 34. [CrossRef]
22. Kim, J.E.; Carosi, G. Axions and the strong *CP* problem. *Rev. Mod. Phys.* **2010**, *82*, 557–601. [CrossRef]
23. Sikivie, P. Invisible axion search methods. *Rev. Mod. Phys.* **2021**, *93*, 015004. [CrossRef]
24. Borsanyi, S.; Fodor, Z.; Guenther, J.; Kampert, K.H.; Katz, S.D.; Kawanai, T.; Kovacs, T.G.; Mages, S.W.; Pasztor, A.; Pittler, F.; et al. Calculation of the axion mass based on high-temperature lattice quantum chromodynamics. *Nature* **2016**, *539*, 69–71. [CrossRef] [PubMed]
25. Gorghetto, M.; Hardy, E.; Villadoro, G. More axions from strings. *SciPost Phys.* **2021**, *10*, 050. [CrossRef]
26. Buschmann, M.; Foster, J.W.; Hook, A.; Peterson, A.; Willcox, D.E.; Zhang, W.; Safdi, B.R. Dark matter from axion strings with adaptive mesh refinement. *Nat. Commun.* **2022**, *13*, 1049. [CrossRef] [PubMed]
27. Hindmarsh, M.; Lizarraga, J.; Lopez-Eiguren, A.; Urrestilla, J. Approach to scaling in axion string networks. *Phys. Rev. D* **2021**, *103*, 103534. [CrossRef]
28. Yamaguchi, M.; Kawasaki, M.; Yokoyama, J. Evolution of Axionic Strings and Spectrum of Axions Radiated from Them. *Phys. Rev. Lett.* **1999**, *82*, 4578–4581. [CrossRef]
29. Braaten, E.; Mohapatra, A.; Zhang, H. Dense Axion Stars. *Phys. Rev. Lett.* **2016**, *117*, 121801. [CrossRef]
30. Braaten, E.; Zhang, H. Colloquium: The physics of axion stars. *Rev. Mod. Phys.* **2019**, *91*, 041002. [CrossRef]
31. Schiappacasse, E.D.; Hertzberg, M.P. Analysis of dark matter axion clumps with spherical symmetry. *J. Cosmol. Astropart. Phys.* **2018**, *2018*, 037. [CrossRef]
32. Visinelli, L.; Baum, S.; Redondo, J.; Freese, K.; Wilczek, F. Dilute and dense axion stars. *Phys. Lett. B* **2017**, *777*. [CrossRef]
33. Jetzer, P. Boson stars. *Phys. Rep.* **1992**, *220*, 163–227. [CrossRef]
34. Eby, J.; Leembruggen, M.; Street, L.; Suranyi, P.; Wijewardhana, L.C.R. Global view of QCD axion stars. *Phys. Rev. D* **2019**, *100*, 063002. [CrossRef]
35. Bautista, B.; Degollado, J.C. Static axion stars revisited. *Front. Astron. Space Sci.* **2024**, *11*, 1346820. [CrossRef]
36. Diez-Tejedor, A.; Marsh, D.J. Cosmological production of ultralight dark matter axions. *arXiv* **2017**, arXiv:1702.02116. [CrossRef]
37. Lee, J.-W. Brief History of Ultra-light Scalar Dark Matter Models. *EPJ Web Conf.* **2018**, *168*, 06005. [CrossRef]
38. Hui, L.; Ostriker, J.P.; Tremaine, S.; Witten, E. Ultralight scalars as cosmological dark matter. *Phys. Rev. D* **2017**, *95*, 043541. [CrossRef]
39. Visinelli, L. Light axion-like dark matter must be present during inflation. *Phys. Rev. D* **2017**, *96*, 023013. [CrossRef]
40. Marsh, D.J.E. Axion cosmology. *Phys. Rep.* **2016**, *643*, 1–79. [CrossRef]
41. Kim, J.E.; Marsh, D.J.E. An ultralight pseudoscalar boson. *Phys. Rev. D* **2016**, *93*, 025027. [CrossRef]
42. Iršič, V.; Viel, M.; Haehnelt, M.G.; Bolton, J.S.; Becker, G.D. First Constraints on Fuzzy Dark Matter from Lyman-α Forest Data and Hydrodynamical Simulations. *Phys. Rev. Lett.* **2017**, *119*, 031302. [CrossRef]
43. Armengaud, E.; Palanque-Delabrouille, N.; Yèche, C.; Marsh, D.J.E.; Baur, J. Constraining the mass of light bosonic dark matter using SDSS Lyman-α forest. *Mon. Not. R. Astron. Soc.* **2017**, *471*, 4606–4614. [CrossRef]
44. Kobayashi, T.; Murgia, R.; De Simone, A.; Iršič, V.; Viel, M. Lyman-α constraints on ultralight scalar dark matter: Implications for the early and late universe. *Phys. Rev. D* **2017**, *96*, 123514. [CrossRef]

45. Wechsler, R.H.; Tinker, J.L. The Connection Between Galaxies and Their Dark Matter Halos. *Annu. Rev. Astron. Astrophys.* **2018**, *56*, 435–487. [CrossRef]
46. Frieman, J.A.; Turner, M.S.; Huterer, D. Dark Energy and the Accelerating Universe. *Annu. Rev. Astron. Astrophys.* **2008**, *46*, 385–432. [CrossRef]
47. Ryden, B. *Introduction to Cosmology*; Cambridge University Press: New York, NY, USA, 2017.
48. Braaten, E.; Mohapatra, A.; Zhang, H. Nonrelativistic Effective Field Theory for Axions. *Phys. Rev.* **2016**, *D94*, 076004, [arXiv:hep-ph/1604.00669]. [CrossRef]
49. Davidson, S.; Schwetz, T. Rotating drops of axion dark matter. *Phys. Rev. D* **2016**, *93*, 123509. [CrossRef]
50. Eby, J.; Mukaida, K.; Takimoto, M.; Wijewardhana, L.C.R.; Yamada, M. Classical nonrelativistic effective field theory and the role of gravitational interactions. *Phys. Rev. D* **2019**, *99*, 123503. [CrossRef]
51. Eby, J.; Suranyi, P.; Vaz, C.; Wijewardhana, L.C.R. Axion Stars in the Infrared Limit. *J. High Energy Phys.* **2015**, *3*, 080, Erratum *J. High Energy Phys.* **2016**, *11*, 134. [CrossRef]
52. Miniati, F.; Gregori, G.; Reville, B.; Sarkar, S. Axion-Driven Cosmic Magnetogenesis during the QCD Crossover. *Phys. Rev. Lett.* **2018**, *121*, 021301. [CrossRef]
53. Planck Collaboration; Aghanim, N.; Akrami, Y.; Arroja, F.; Ashdown, M.; Aumont, J.; Baccigalupi, C.; Ballardini, M.; Banday, A.J.; Barreiro, R.B.; et al. Planck 2018 results—I. Overview and the cosmological legacy of Planck. *Astron. Astrophys.* **2020**, *641*, A1. [CrossRef]
54. Binney, J.; Tremaine, S. *Galactic Dynamics*; Princeton University Press: Princeton, NJ, USA, 2011.
55. Schive, H.Y.; Chiueh, T.; Broadhurst, T. Cosmic structure as the quantum interference of a coherent dark wave. *Nat. Phys.* **2014**, *10*, 496–499. [CrossRef]
56. Schive, H.Y.; Liao, M.H.; Woo, T.P.; Wong, S.K.; Chiueh, T.; Broadhurst, T.; Hwang, W.Y.P. Understanding the Core-Halo Relation of Quantum Wave Dark Matter from 3D Simulations. *Phys. Rev. Lett.* **2014**, *113*, 261302. [CrossRef] [PubMed]